Engineering Structures 315 (2024) 118369

Contents lists available at ScienceDirect

Engineering Structures

journal homepage: www.elsevier.com/locate/engstruct

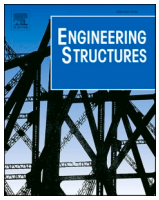

A simplified model for rocking panels with friction connections

Emanuele Gandelli [a,*], Marco Lamperti Tornaghi [b], Dionysios Bournas [b]

[a] Department of Civil, Environmental, Architectural Engineering and Mathematics (DICATAM), University of Brescia, Italy
[b] European Commission. Joint Research Centre (JRC), Ispra, Italy

ARTICLE INFO

Keywords:
Analytical model
Self-centring structures
Displacement-based design
Friction connection
Rocking panel

ABSTRACT

In recent decades, various rocking systems have been proposed to enhance the self-centring capacity of structures after seismic events. Sometimes dissipative devices have been added to control peak lateral displacements. However, the computational models currently available in the literature are not suitable for practitioners because they require the solution of complex differential equations describing the negative tangent stiffness that characterises the intrinsic instability of rocking motion. To address this issue, this study explores a simplified model for rocking panels with panel-to-panel friction connections, potentially combined with moment-resisting frames. The remarkable sliding stiffness of these connections enables to simulate the system as a SDOF oscillator adapting original Displacement-Based Design (DBD) procedures, without the need to resort to closed-form solutions. The accuracy of the model is validated by comparing its results to pseudo-dynamic tests on a precast industrial building reported in the literature.

1. Introduction

The performance of structures subjected to strong earthquakes is usually achieved by developing significant inelastic deformations to dissipate energy in a controlled manner within their critical regions, such as plastic hinges at column bases and beam-to-column connections. This often leads to permanent deformations and residual displacements. Practical experience and previous research have shown that overcoming relatively low levels of residual drift leads to difficult and uneconomic repair of a structure [e.g., [3,40,42]]. This may even result in the demolition of the building. Business interruption significantly increases the total economic loss resulting from the demolition of a building after an earthquake, but above all, it creates significant social and economic disruptions that worsen the resilience by slowing down the recovery of earthquake-affected communities.

Earthquake engineering research in recent decades has focused on rapid recovery by drastically reducing displacements and residual deformations of structures, leading to two primary approaches: *base isolation* and *self-centring* structures. Seismic *base isolation* decouples a superstructure from the foundation, laid on the shaking ground, to reduce the seismic demands on the isolated superstructure with its non-structural elements [e.g., [30]]. The complexity of the design lies in the system to decouple the foundation and the superstructure, which may also undergo significant displacements that do not affect its ultimate integrity. The resulting building could be designed as if it were in a low seismic area.

The idea of incorporating elastic restraints capable of withstanding large deformations (displacements) without loss of mechanical properties became popular in the 1990s, starting with bridges and precast concrete structures [14,34]. Once the earthquake has occurred, these internal constraints are able to restore the structure to its original condition. Structural elements, such as beam-to-column connections, are free to rotate rigidly by concentring deformation in gap opening and closure controlled by Post-Tensioned (PT) tendons that act as springs to ensure self-restoring capability. Then, many scholars refer to this approach as *self-centring* [42]. It has become more popular in the US and NZ, spanning from prefabricated structures to other types of construction, sometimes replacing PT tendons, originally used as elastic internal constraints, with other systems (shape memory alloys, springs, etc.).

Alternatively, a synthesis of the previous two approaches could be pursued to respond to the ground motion excitation: either allow the structure to uplift from its foundation level or rock. Structures fastened to the ground, using foundation systems that prevent uplift and sliding, dominate modern seismic design, but the good performance in earthquakes of modern and ancient buildings that were unintentionally designed to rock has led engineers to investigate uplift and rocking as a

* Corresponding author.
E-mail address: emanuele.gandelli@unibs.it (E. Gandelli).

https://doi.org/10.1016/j.engstruct.2024.118369
Received 11 September 2023; Received in revised form 4 May 2024; Accepted 2 June 2024
Available online 20 June 2024

technique for modifying the seismic response of structures. Uplift at the interface between rocking members acts as a mechanical fuse, limiting the forces transmitted to the structure; see [3,40,42] for a detailed review.

As the base isolation enables mutual sliding with the foundation, the rocking causes uplift and gap opening. Again, the result is a re-centring system, but no additional devices are required for elastic forces, as the gravitational load itself provides the self-centring action. After the first pioneering attempts to study swinging structures, in 1963, Housner proved analytically that of two geometrically similar blocks, the larger one is more stable when dynamically excited [20]. Accordingly, ground motions with longer dominant periods have a greater overturning potential. In displacement-based design terminology, larger blocks have a greater *displacement capacity* [3]. An iconic archetype of pure rocking structures, with relevant geometric parameters, is shown in Fig. 1-a,b. According to some Authors [e.g., [23,36]], these rocking blocks have a more stable behaviour than isolated ones featuring the same base (i.e., b) and height (i.e., h) since the weight (i.e., mg) of the roof beam increases stability and provides a higher self-centring force. A key parameter governing the moment-rotation response of pure rocking structures is the *slenderness angle* $\theta = \arctan(b/h)$. Indeed, as shown in Fig. 1-d, as long as the seismic lateral loads does not trigger the uplift moment $M_{up} = (mgR)\sin\theta$, the block experiences very small elastic flexural deformations (associated the stiffness k_1). Then, once the block is rocking (see Fig. 1-c), its rotational stiffness (i.e., k_2) becomes negative until the resisting moment of the gravity load becomes null when the *rotation angle* α is equal to θ [23].

An overview of the different solutions proposed in the last decades to improve the seismic response of pure rocking systems inserted in moment-resisting frames is provided in Fig. 2. In first studies [24,25], simple precast walls were equipped with unbonded post-tensioned tendons acting as elastic restrains (see Fig. 2-a); these enable to overcome the intrinsic instability of rocking systems by increasing the secondary slope (i.e., k_2). To increase damping, dissipative connections can be installed either along the tendons [2], at the panel base [15,18,19] or in the joints with the frame (see Fig. 2-b). Alternatively, the panels can be locked at the base ends with shear keys (see Fig. 2-c) that prevent them from sliding but allow them to be lifted and rocked (stepping rocking) [1,4,22,27]. Other solutions provide rocking panels devoid of elastic restraints but, as in the previous cases, an increased damping using dissipative connections to connect frame (see Fig. 2-c) or foundations [6,26,38] (see Fig. 2-d). Conversely, pin-supported walls (see Fig. 2-e), where gravity does not contribute to stability, cannot stand without a parallel frame, but can improve the damping of the whole system by using friction connections [17,37,39].

While several solutions have been proposed, it is still a challenge for engineers and practitioners to predict the lateral response of dissipative rocking structures under severe seismic excitations using simple tools. The existing models, including those developed by Christopoulos et al. [10] and Aghagholizadeh & Makris [1], Zhong and Christopoulos [42], require solving complex second-order differential equations. According to Makris and Konstantinidis [28], the simple design method, using equivalent elastic characteristics and a response-spectra approach, proposed by Priestley et al. [33] may not be appropriate for structures lacking a dual frame system or supplemental dissipative devices.

This study presents a simplified design model for rocking panels with friction connections, which is based on the original Displacement-Based Design (DBD) procedures developed by Priestley et al. [35]. Rocking panels and friction dampers can be used in connection with a moment-resisting frame (as shown in case 'c' of Fig. 2) or independently. Friction connections provide damping with a significant force-displacement sliding stiffness, capable of compensating for the negative secondary slope associated with rocking motion.

The effectiveness and accuracy of the proposed calculation model are validated against the results of pseudo-dynamic tests carried out in a previous study by the Authors [31].

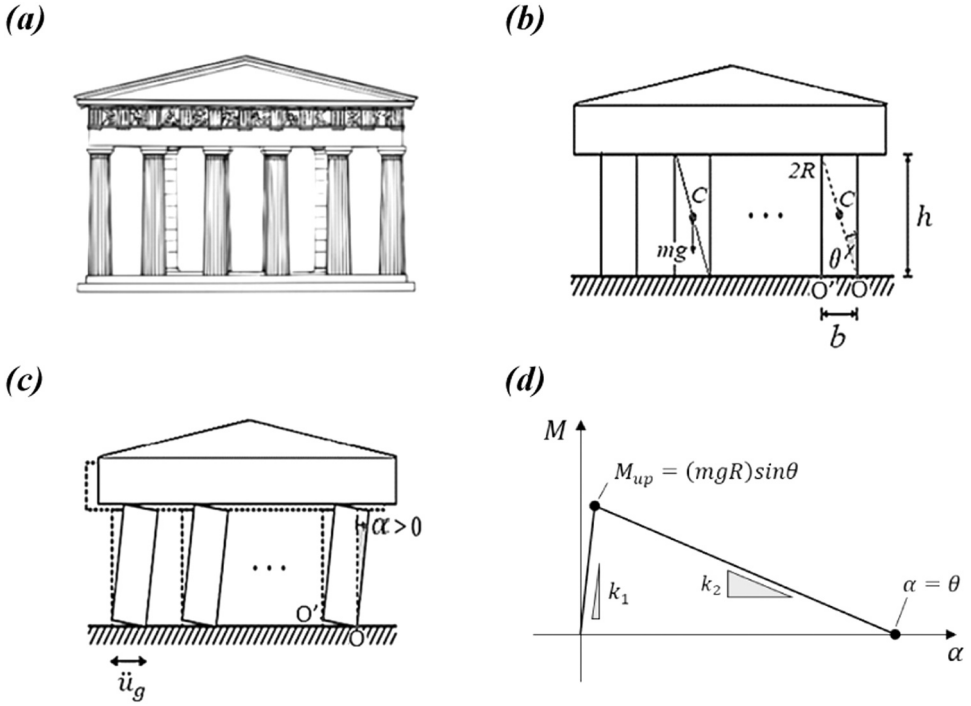

Fig. 1. Archetype of a pure rocking structure: (a) initial undeformed position and (b) main geometric parameters; (c) rocking deformed configuration; (d) moment - rotation response.

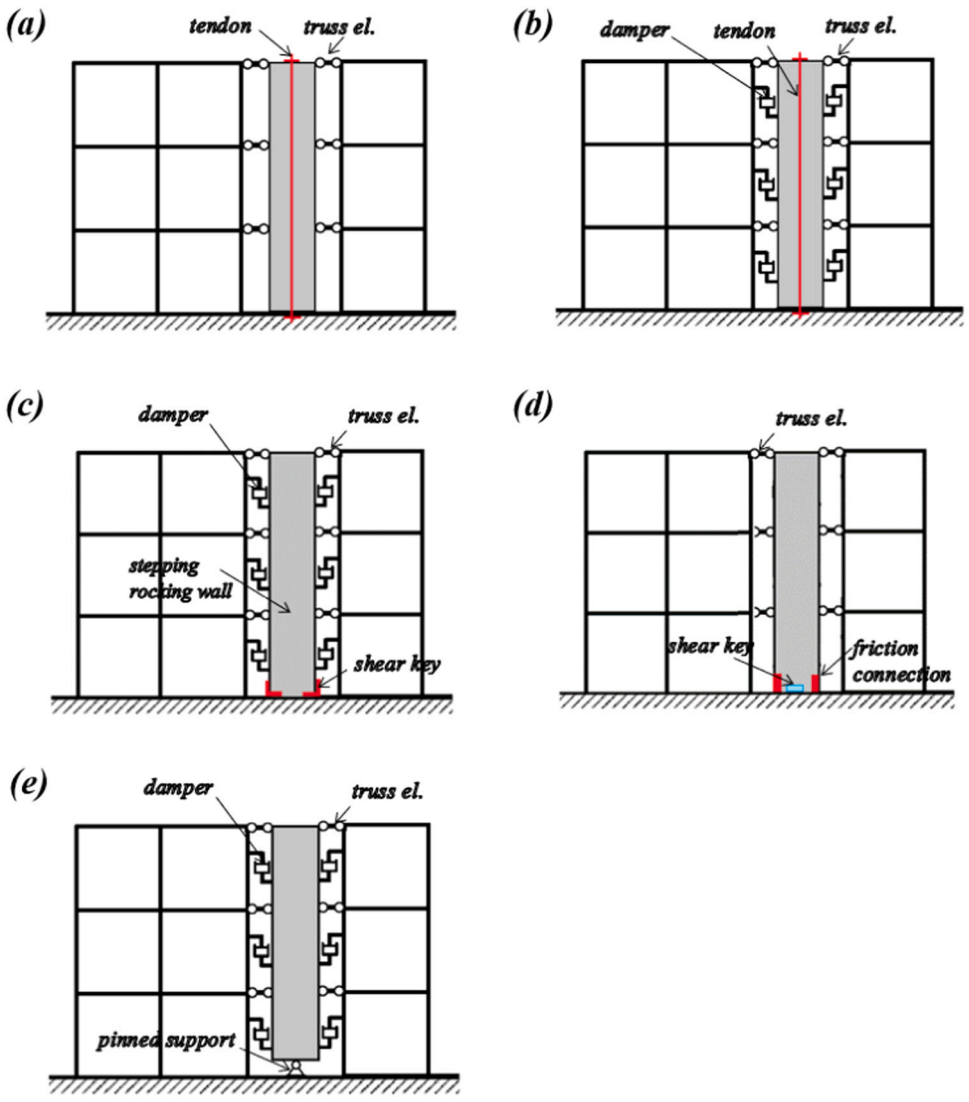

Fig. 2. Layouts of rocking panels in combination with moment-resisting frames with different self-centering systems: (a) elastic restraints tendons only; (b) elastic restraints tendons with dissipative connections; (c) stepping rocking panel with dissipative connections to frame and (d) to foundation; (e) pinned-supported walls with dissipative connections.

2. Rocking panels with friction connections

Some scholars addressed the seismic strengthening of buildings using dissipative rocking panels. Among these solutions, two different structural schemes can be identified: heavy concrete panels are connected to the main frame (either made of R.C. or steel) through a horizontal shear connector, as shown in Fig. 3-a, [4,6,31]. The second is more suitable for lighter timber buildings made of CLT panels that take both horizontal and vertical loads, as in Fig. 3-b, [8,26,41]. In both cases, the rocking motion of the panels is achieved by constraining the corners at the base of the panels using shear keys (highlighted in blue in Fig. 3), which alternatively act as hinges depending on the direction of motion [26].

The upper panel connection, again in blue in Fig. 3, links the top edge to the beam to transmit lateral seismic loads. The second scheme uses

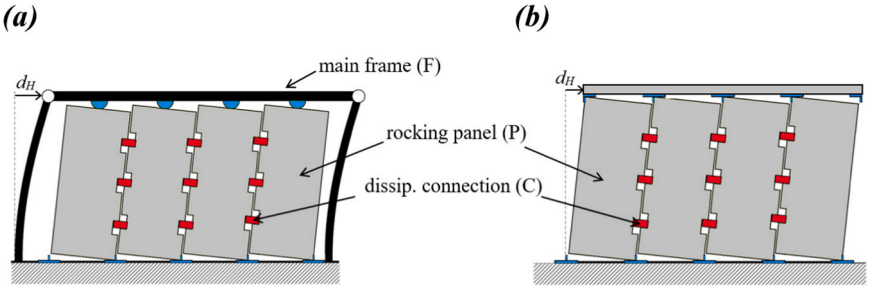

Fig. 3. Layouts for dissipative rocking panels installed in buildings with (a), i.e., scheme-1 or (b) without, i.e., scheme-2, a main resisting frame. Adapted from [31].

the same connection to transfer also the gravity load of the top slab, resulting in a higher lateral stiffness of the rocking panels. Dissipative friction connections, highlighted in red in Fig. 3, link the vertical edges of adjacent panels to increase the overall damping of the structural systems in both schemes, see Fig. 9 for more information on these connections. During the rocking motion, the relative vertical displacement between panels triggers energy dissipation within the connections. These can be designed to exploit friction loads or the yielding of some sacrificial (and replaceable) metallic components.

3. Simplified model for seismic calculations

The overall lateral response of single-storey buildings equipped with dissipative rocking panels can be estimated through a linear equivalent spectral analysis (Fig. 4-b) that, depending on the adopted structural scheme, employs two or three "spring-dashpot" systems arranged in parallel (Fig. 4-a). For the sake of clarity, hereafter in the paper, the quantities with subscripts "F", "P", and "C" will be applied to the mechanical properties of the main frame (F), the panels (P), and the connections (C), respectively. Obviously, when performing the spectral analysis for the second structural scheme all the quantities of the main frame (subscripts "F") must be neglected.

The effective vibration period (T_{eff}) of the considered structural system is:

$$T_{eff} = 2\pi\sqrt{\frac{m_1}{(k_{F,eff} + k_{P,eff} + k_{C,eff})}} \tag{1}$$

being: (i) m_1 the modal mass of the fundamental mode shape; (ii) $k_{F,eff}$, $k_{P,eff}$, and $k_{C,eff}$ the effective stiffness in the horizontal direction of the main frame, the rocking panels, and the dissipative connections, respectively.

In accordance with [35] for "in parallel systems", the overall equivalent viscous damping (ξ_{eq}) is:

$$\xi_{eq} = \xi_{el,F} + \frac{(\xi_{F,eq} \bullet F_{F,\max} + \xi_{P,eq} \bullet F_{P,\max} + \xi_{C,eq} \bullet F_{C,\max})}{(F_{F,\max} + F_{P,\max} + F_{C,\max})} \tag{2}$$

being: (i) $\xi_{el,F}$ the viscous damping of the main frame in the elastic range (here conventionally assumed equal to 5 %); (ii) $\xi_{F,eq}$, $\xi_{P,eq}$, and $\xi_{C,eq}$ the equivalent viscous damping offered by the main frame, the rocking panels, and the dissipative connections, respectively, when operating beyond their elastic regime; (iii) $F_{F,\max}$, $F_{P,\max}$, and $F_{C,\max}$ are the forces (horizontal components) at the maximum displacement amplitude developed by the main frame, the rocking panels, and the dissipative connections, respectively.

The mechanical properties of the main frame (made either of reinforced concrete or steel elements) can be obtained from a pushover analysis. Indeed, the relevant capacity curve (i.e. a plot of base-shear vs. roof displacement) can be bi-linearised (Fig. 5) exploiting the "equal energy criterion" of the EC8-Annex B [9], allowing the identification of a yielding force ($F_{F,y}$) and displacement ($d_{F,y}$). It is worth noting that, since the frame considered in this study forms a single storey (i.e. SDOF system), the participation factor of the fundamental mode shape is $\Gamma_1 = 1.0$ and, therefore, does not generate any effect when scaling the capacity curve ($F/\Gamma_1 = F$, and $d/\Gamma_1 = d$).

From the equivalent bilinear plot, it is possible to calculate the effective stiffness of the main frame ($k_{F,eff}$):

$$k_{F,eff} = F_{F,y}/d_{H,\max} \tag{3}$$

being $d_{H,\max}$ the maximum lateral displacement experienced at roof level during the shaking ground motion. The equivalent viscous damping ($\xi_{F,eq}$) can be calculated through the equations proposed in [5]:

$$\xi_{F,eq} = \begin{cases} \frac{95}{\pi} \bullet \left(1 - \frac{1}{\sqrt{\mu_F}}\right) \bullet \left(1 + \frac{1}{(T_{eff} + 0.85)^4}\right) \bullet \left(1 + \frac{1}{1.35^4}\right)^{-1} & \text{for r.c. frames (with } \mu_F \geq 1) \\ \frac{140}{\pi} \bullet \left(1 - \frac{1}{\sqrt{\mu_F}}\right) \bullet \left(1 + \frac{1}{(T_{eff} + 0.85)^2}\right) \bullet \left(1 + \frac{1}{1.35^2}\right)^{-1} & \text{for steel frames (with } \mu_F \geq 1) \\ 0 & \text{in any case when } \mu_F < 1 \end{cases} \tag{4}$$

being μ_F the ductility demand on the main frame:

$$\mu_F = d_{H,\max}/d_{F,y} \tag{5}$$

Usually, in practical design applications, the linear equivalent spectral procedure is iterative. First, the structural engineer establishes a

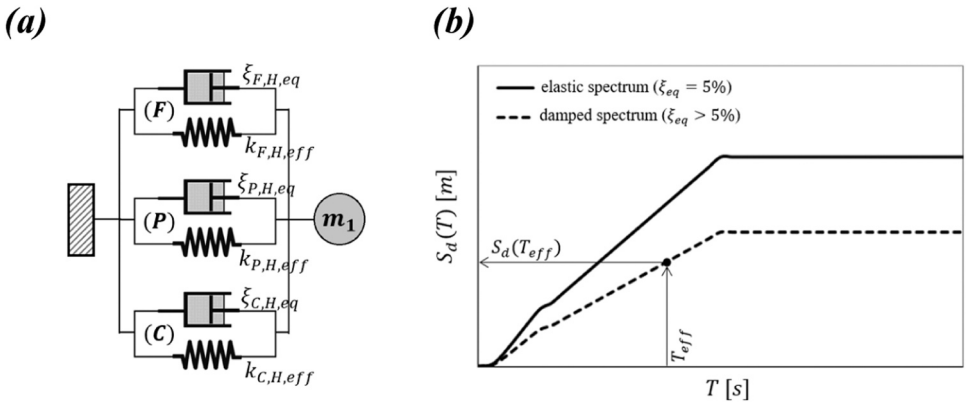

Fig. 4. Adopted calculation method: (a) mass-spring-dashpot model; (b) displacement response spectrum analysis.

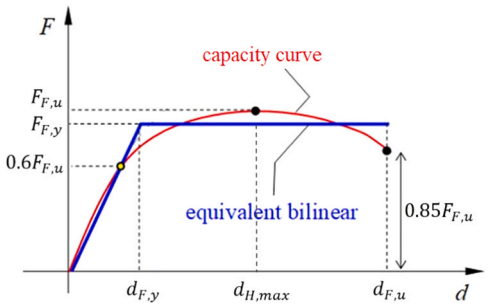

Fig. 5. Definition of the equivalent elastic-perfectly system of the main frame according to EC8 [9].

target displacement ($d_{targ} = d_{H,\max}$) within two possible ranges [13,16,32]: (1) $d_{targ} \le d_{F,y}$ when the goal is to maintain the main frame in the elastic range; (2) $d_{F,y} < d_{targ} < d_{F,u}$ when a certain plastic excursion is accepted. Eventually, assuming that the geometry and typology of the rocking panel is given (e.g., from manufacturer data sheet or tested in lab), the dissipative force offered by the connection ($F_{C,y}$) is varied until the convergence is attained:

$$\left|S_d\left(T_{eff}\ ,\ \xi_{eq}\right) - d_{targ}\right| \le toll \tag{6}$$

where *toll* is a small tolerance threshold (e.g. $toll = 1\%\ d_{targ}$), and the damped spectral displacement $S_d\left(T_{eff},\ \xi_{eq}\right)$ is calculated from the relevant elastic value $S_d\left(T_{eff},\ \xi_{el} = 5\%\right)$ though the reduction factor η proposed in [35]:

$$\begin{cases} S_d\left(T_{eff}, \xi_{eq}\right) = \eta \bullet S_d\left(T_{eff}, \xi_{el} = 5\%\right) \\ \eta = \sqrt{7/(2+\xi_{eq})} \end{cases} \tag{7-a,b}$$

It is worth noting that Eq. 4 overcomes the inherent error of more conventional approaches based on the Jacobsen formulation [21] that typically overestimate the equivalent damping ratio of medium-to-long period hysteretic systems [29]. Moreover, it was found that the proposed approach, in combination with the adopted spectral reduction factor (Eq. 7-b), guarantees the best accuracy in the prediction of peak displacements of a wide range of inelastic systems [7].

The contribution of each of the dissipative rocking panels to the overall dynamic response of the considered structural system can be estimated through the analytical model developed hereafter. In this regard, referring to the dynamic equilibrium of a panel plus the dissipative connections ("P + C") shown in Fig. 6: (1) O is the pivot or hinge point of the rocking panels (usually realised through a shear key); (2) P is the "control point". In the structural "scheme-1″ (Fig. 6-a), P is located in the middle of the upper edge of the panel and transmits horizontal inertia loads, only. In the "scheme-2″ (Fig. 6-b), P is located at one of the top corners of the panel and takes also the vertical load coming from the upper slab (W_S); (3) b and h are the width and the height of the panel, respectively; (4) W_P is the self-weight of the panel; (5) F_{P+C} is the horizontal load causing the rocking movement (equal to the shear force at the base of the panel); (6) F_C is the damping force developed within the dissipative connection; (7) α is the rotation of the panel about the "hinge point".

The horizontal displacement (d_H) at the "control point" P is related to the rotation angle through this equation:

$$d_H = \begin{cases} h\sin\alpha + b(1-\cos\alpha)/2 & \text{for scheme 1} \\ h\sin\alpha + b(1-\cos\alpha) & \text{for scheme 2} \end{cases} \tag{8}$$

Analogously, the vertical displacement at the base of the panel (d_V) is:

$$d_V = b\sin\alpha \tag{9}$$

For a single dissipative rocking panel, the equilibrium of moments about the "pivot point" is ($W_S = 0$ for "scheme 1"):

$$F_{P+C} \bullet h' = W_P \bullet b'_P + W_S \bullet b'_S + F_C \bullet b \rightarrow F_{P+C} = \frac{W_P \bullet b'_P + W_S \bullet b'_S + F_C \bullet b}{h'} \tag{10}$$

where h' is the lever arm of the seismic force (F_{P+C}) in the deformed configuration of the panel:

$$h' = h'(\alpha) = \begin{cases} (b\ sin\ \alpha)/2 + h\ cos\ \alpha & \text{for scheme 1} \\ b\sin\alpha + h\ cos\ \alpha & \text{for scheme 2} \end{cases} \tag{11}$$

while b'_P and b'_S are the lever arms, in the deformed configuration of the panel, of the vertical loads W_P and W_S, respectively:

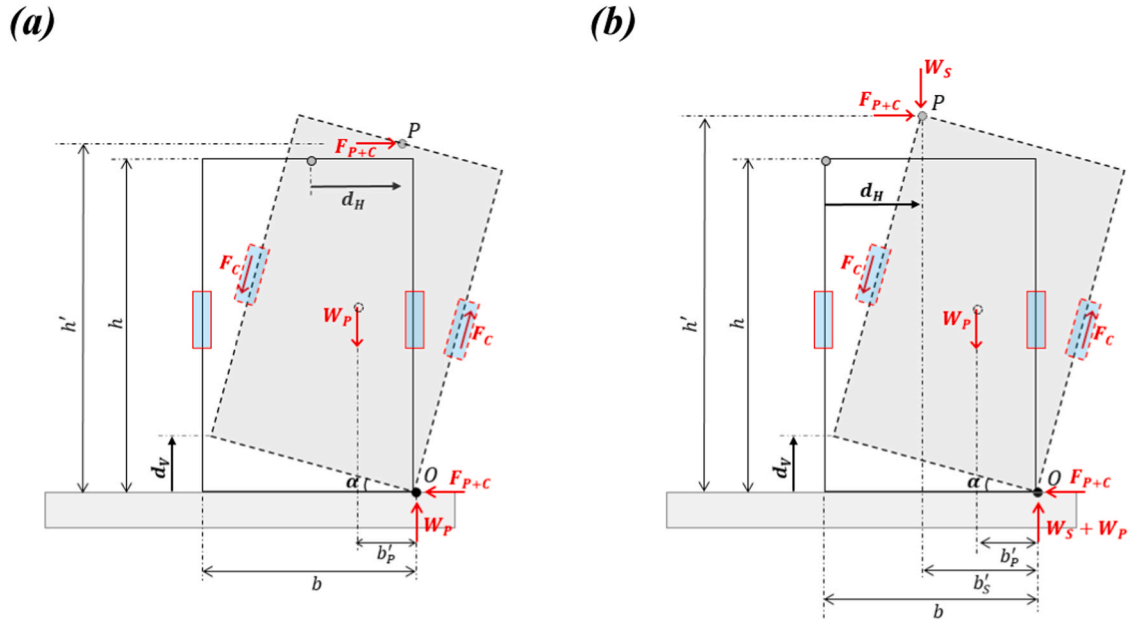

Fig. 6. Rocking panel with dissipative connections: (a) "installation scheme-1″, more suitable to r.c. or steel frames; (b) "scheme-2″, more suitable to timber buildings.

$$b'_P = b'_P(\alpha) = (b\cos\alpha - h\sin\alpha)/2 \tag{12}$$

$$b'_S = b'_S(\alpha) = b\cos\alpha - h\sin\alpha \tag{13}$$

It is worth noting that the overall resisting force (F_{P+C}) offered by the system along the horizontal direction (relevant quantities hereafter referred with the subscript "H") can be seen as:

$$F_{P+C} = F_{P,H} + F_{C,H} \tag{14}$$

being $F_{P,H}$ the contribution to the equilibrium of moments due to the vertical loads only ($W_S = 0$ for "scheme 1″):

$$F_{P,H} = \left(W_P \bullet b'_P + W_S \bullet b'_S\right)/h' \tag{15}$$

and $F_{C,H}$ the contribution generated by the dissipative force (F_C) developed within the connection:

$$F_{C,H} = F_C \bullet b/h' \tag{16}$$

More in general, for a series of rocking panels aligned to constitute a cladding wall (as shown in Fig. 3) the equilibrium of forces equation becomes:

$$F_{P+C} = n_p \bullet F_{P,H} + n_c \bullet F_{C,H} \tag{17}$$

being n_p the number of panels forming the wall (e.g., $n_p = 4$ for the case shown in Fig. 3), and n_c the number of dissipative connections generating a resisting moment against rotations (e.g., $n_c = 9$ for the case shown in Fig. 3). For the sake of clarity, it is important to note that the proposed analytical model relies on the following assumptions:

1. the "pivot-type" rotation point is devoid of a smeared compression zone;
2. the rocking motion does not damage panel edges. In fact, dissipative connections limit the upward rise and brake the descent of panels, reducing their impact on the ground;
3. although the model may take into account the plasticisation of the resisting frame, it will not be validated for it. Indeed, in the reference experimental tests (see Section 4) the frame remained in the elastic range. This is in line with good design practices: activating the friction devices prevents damage caused by lateral loads to the frame structure (when present);
4. the Displacement-Based-Design (DBD) calculation tool may have poor accuracy for very stiff structures with periods lower than 0.30 s. Conversely, it has been proven to be reliable for mid to long period bridge structures [7] and for reinforced concrete or steel frames with fundamental periods ranging from 0.30 s to 2.0 s as in this research [16].

3.1. Lateral strength of bare rocking panels

In this Section, the contribution of the bare rocking panels (i.e. without dissipative connections) to the lateral strength and stiffness of the whole structural system (Fig. 3) is discussed. In this regard, the horizontal force generated at the control point by the rocking panels depends on the amplitude of the displacement (d_H) and obeys to a bilinear and reversible force-displacement relationship shown in Fig. 7. Before the activation of the rocking movement, the response of the panel is governed by its elastic flexural stiffness ($k_{P,H,1} = k_{P,H,el}$) that allows the introduction of the relevant (apparent) "yielding displacement" ($\tilde{d}_{P,H,y}$). The breakaway force ($\tilde{F}_{P,H,y}$) that is necessary to trigger the first rotation of the panel can be approximated as ($W_S = 0$ for "scheme 1″):

$$\tilde{F}_{P,H,y} \cong \frac{b(W_P/2 + W_S)}{h} \tag{18}$$

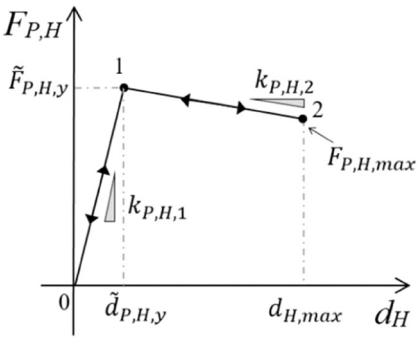

Fig. 7. Force-displacement response of rocking panels without connections.

After the breakaway, the lateral strength of the panel tends to decrease generating a negative "post-yielding" slope ($k_{P,H,2} < 0$). Indeed, as shown in Fig. 6, for higher displacements the lever arms of the vertical loads W_P (i.e., b'_P), and W_S (i.e., b'_S) tend to decrease while, on the contrary, that of F_P (i.e., h') tends to increase. At the maximum displacement ($d_{H,\max}$) the lateral strength ($F_{P,H,\max}$) of the panel is ($W_S = 0$ for "scheme 1″):

$$F_{P,H,\max} = \left[W_P \bullet b'_{P,\alpha_{\max}} + W_S \bullet b'_{S,\alpha_{\max}}\right] \Big/ h'_{\alpha_{\max}} \tag{19}$$

being: $b'_{P,\alpha_{\max}} = b'_P(\alpha_{\max})$, $b'_{S,\alpha_{\max}} = b'_S(\alpha_{\max})$, and $h'_{\alpha_{\max}} = h'(\alpha_{\max})$.

It is worth noting that, since in the unloading the same bilinear response is retraced (with opposite direction), the panels do not offer any energy dissipation capacity. Therefore, the linear equivalent dynamic properties, i.e. effective stiffness ($k_{P,H,eff}$) and equivalent viscous damping ($\xi_{P,H,eq}$), are:

$$\begin{cases} k_{P,H,eff} = F_{P,H,\max}/d_{H,\max} \\ \xi_{P,H,eq} = 0\% \end{cases} \tag{20}$$

3.2. Lateral strength due to friction connections

In this Section, the contribution of the dissipative connections to the overall lateral stiffness and damping of the whole structural system (Fig. 3) is discussed. In particular, for sake of brevity, only friction connections will be considered since experimental evidences [11] proved that they are characterised by a pronounced positive slope in the first and third quadrants, useful to counterbalance the negative slope after rocking. This does not limit the range of validity of the proposed model since "yielding connections" featuring an elastic perfectly plastic response are covered by the more general model presented hereafter. In this regard, for the sake of simplicity, the relative displacement occurring within adjacent friction connections is approximated with the vertical displacement at the base of the panel (d_V). The force-displacement response of the friction connections is shown qualitatively in Fig. 8-a. At the motion breakaway, the connection develop a resisting force F_C equal to $F_{C,0}$ while a sort of "hardening effect" with slop equal to $k_{C,2}$ can (not always) be appreciated for higher displacement amplitudes until the maximum force ($F_{C,\max}$) is reached:

$$F_{C,\max} = F_{C,0} + k_{C,2} \bullet d_{V,\max} = F_{C,0} + k_{C,2} \bullet b \bullet \sin\alpha_{\max} \tag{21}$$

This formula is based on the results of a wide experimental campaign carried out to characterise some prototypes of friction connection for dissipative panels [11]. An example of these connections is shown in Fig. 9-a,b,c with the relevant recorded hysteretic loops reported in Fig. 9-d. In line with the design targets, the connections exhibit a remarkable sliding (tangent) stiffness $k_{C,H,2} \cong 0.9kN/mm$. This stiffness has a beneficial effect on stabilising the rocking motion of panels.

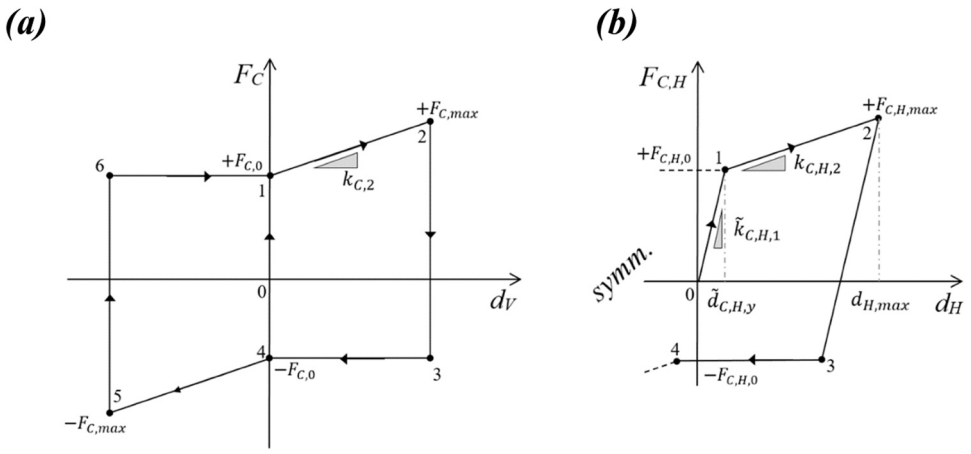

Fig. 8. Hysteretic response of the dissipative friction connections: (a) force vs. vertical relative displacement among the adjacent panels; (b) force vs. horizontal displacement at the control point.

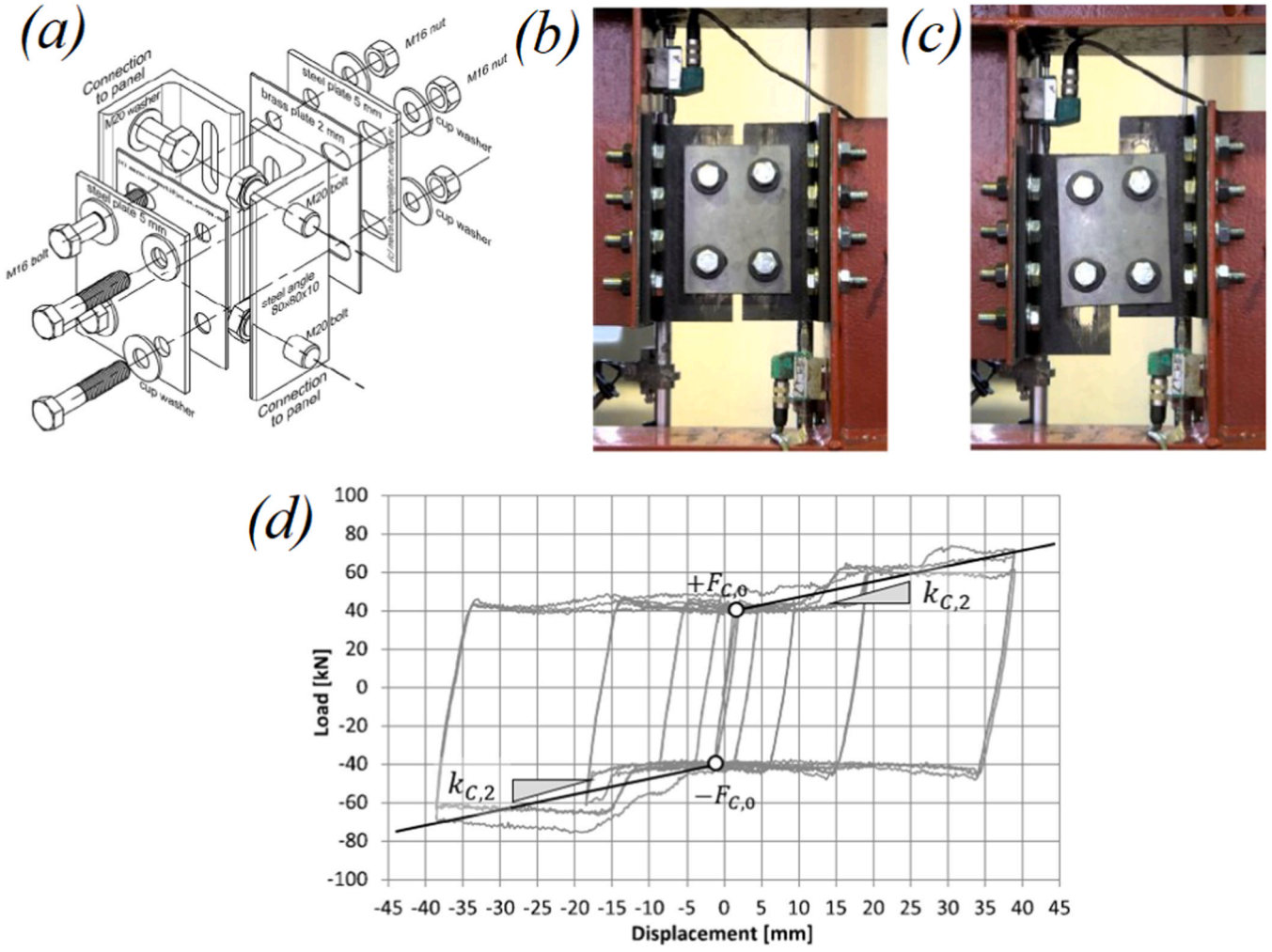

Fig. 9. Prototype of friction connection for dissipative panels [11]: (a) components in axonometric view; (b) device assembly for characterisation tests; (c) device under the maximum drift; (d) recorded hysteretic loops.

Due to the intrinsic nature of friction connections, the elastic stiffness of the system that precedes the sliding motion theoretically is very high (theoretically tends to infinite). However, for the calculation of the effective damping offered by the connection (related to the achieved ductility level), it is convenient to refer to the horizontal component ($F_{C,H}$, see the previous Section) as a function of the horizontal displacement (d_H) of the control point P (Fig. 8-b). Within this framework, the hysteretic response of the connection is altered by the elastic flexural deformations ($k_{P,H,el}$) of the panel and a kind of apparent elastic stiffness of the connection ($\tilde{k}_{C,H,1} = k_{P,H,el}$) is introduced allowing the definition of the relevant (apparent) "yielding displacement" ($\tilde{d}_{C,H,y}$):

$$\widetilde{d}_{C,H,y} = F_{C,0} \Big/ \widetilde{k}C, H, 1 \tag{22}$$

The maximum amplitude of $F_{C,H}$ can be calculated as:

$$F_{C,H,\max} = F_{C,\max} \bullet (b/h') \tag{23}$$

Or alternatively:

$$F_{C,H,\max} = F_{C,H,0} + k_{C,H,2} \bullet \left(d_{H,\max} - \widetilde{d}_{C,H,y}\right) \tag{24}$$

being $d_{H,\max}$ the maximum horizontal displacement at the "control point" P (obtained through Eq. 8 for $\alpha = \alpha_{\max}$), $F_{C,H,0}$ the strength at motion breakaway, and $k_{C,H,2}$ the "post-yielding" slope:

$$F_{C,H,0} = F_{C,0} \bullet (b/h') \tag{25}$$

$$k_{C,H,2} = \frac{(b/h') \bullet \left(F_{C,\max} - F_{C,0}\right)}{\left(d_{H,\max} - \widetilde{d}_{C,H,y}\right)} \tag{26}$$

The effective stiffness offered by the connections in the horizontal direction ($k_{C,H,eff}$) is:

$$k_{C,H,eff} = F_{C,H,\max} / d_{H,\max} \tag{27}$$

The equivalent viscous damping can be estimated through the analytical expression proposed in [5] for elasto-plastic systems:

$$\xi_{C,H,eq} = \begin{cases} \dfrac{140}{\pi} \bullet \left(1 - \dfrac{1}{\sqrt{\mu_C}}\right) \bullet \left(1 + \dfrac{1}{\left(T_{eff} + 0.85\right)^2}\right) \bullet \left(1 + \dfrac{1}{1.35^2}\right)^{-1} & \text{when } \mu_C \geq 1.0 \\ 0 & \text{when } \mu_C < 1.0 \end{cases} \tag{28}$$

being $\mu_C = d_{H,\max}/\widetilde{d}_{\mu,H,y}$ the (apparent) ductility demand on the dissipative connection. Concerning the application of Eq.(28) to this specific case, it is worth noting that: (1) besides the ductility demand (μ_C), the effective vibration period (T_{eff} regulated by the overall secant stiffness of the system - see Eq. (1)) plays an important role in the definition of the equivalent viscous damping of the connections ($\xi_{C,H,eq}$); (ii) the length of the slotted holes (see Fig. 9(a)), limiting the ductility capacity of the friction plates, may be adjusted to act as a stopper that prevent the exceedance of the ultimate deformation capacity of the frame (i.e., $d_{targ} < d_{F,u}$, see Section 3), if present; (iii) the accuracy and suitability of DBD models have been recently demonstrated also for friction based systems [12] that are intrinsically characterized by high ductility ratios ($\mu > 6$).

3.3. Overall response of the rocking panels with the dissipative connections

The overall response of the rocking panels equipped with the dissipative friction connections can be obtained exploiting the effect superimposition of the two contributions. The result is a "flag shaped" hysteretic loop whose formulae to calculate the point-to-point force-displacement coordinates ($d_H - F_{P+C}$) are given in Table 1. In this regard, for sake of clarity, the point number (e.g., point "1″) is at subscript of both coordinates (e.g., $d_1 - F_1$).

As shown in Fig. 10, by varying the properties of the panels and dissipative connections, four different cases can be distinguished:

Case (a). the system is not self-centring since at the inversion of the motion offers a significant residual strength, i.e., $F_3 < 0$ and $F_4 < 0$. This is due to the fact that the friction force offered within the connection is higher than the re-centring force offered by the panels, i.e. at point 3 $\left(n_c \bullet F_{C,0} \bullet b\right) > n_p \bullet \left(W_P \bullet b'_{P,\alpha_{\max}} + W_S \bullet b'_{S,\alpha_{\max}}\right)$, and at point 4 $\left(n_c \bullet F_{C,0} \bullet b\right) > n_p \bullet \left(W_P \bullet b'_{P,\alpha=0} + W_S \bullet b'_{S,\alpha=0}\right)$;.

Case (b). the system is self-centring since at the inversion of the motion offers a significant re-centring force, i.e., $F_3 > 0$ and $F_4 > 0$. This is due to the fact that the friction force offered within the connection is lower than the re-centring force offered by the panels, i.e. at point 3 $\left(n_c \bullet F_{C,0} \bullet b\right) < n_p \bullet \left(W_P \bullet b'_{P,\alpha_{\max}} + W_S \bullet b'_{S,\alpha_{\max}}\right)$, and at point 4 $\left(n_c \bullet F_{C,0} \bullet b\right) < n_p \bullet \left(W_P \bullet b'_{P,\alpha=0} + W_S \bullet b'_{S,\alpha=0}\right)$;.

Case (c). the system is self-centring and auto-equilibrated since at the inversion of the motion offers a null residual strength, i.e., $F_3 \cong 0$ and $F_4 = 0$. This is due to the fact that the friction force offered within the connection is equal to the re-centring force offered by the panels, i.e. at point 3 $\left(n_c \bullet F_{C,0} \bullet b\right) \cong n_p \bullet \left(W_P \bullet b'_{P,\alpha_{\max}} + W_S \bullet b'_{S,\alpha_{\max}}\right)$, and at point 4 $\left(n_c \bullet F_{C,0} \bullet b\right) = n_p \bullet \left(W_P \bullet b'_{P,\alpha=0} + W_S \bullet b'_{S,\alpha=0}\right)$. This also maximises the dissipation capacity of the connection without compromising self-centring;.

Table 1
Point-to-point force-displacement coordinates of the hysteretic loop of rocking panels with dissipative connections.

point	d_H	F_{P+C}
1	$d_1 = (\widetilde{F}_{P,H,y} + \widetilde{F}_{C,H,y})/k_{P,H,1}$	$F_1 = \dfrac{n_p \bullet \left(W_P \bullet b'_{P,\alpha=0} + W_S \bullet b'_{S,\alpha=0}\right) + n_c \bullet \left(F_{C,0} \bullet b\right)}{h'_{\alpha=0}}$
2	$d_2 = d_H(\alpha_{\max}) = d_{H,\max}$ (see Eq. 8)	$F_2 = \dfrac{n_p \bullet \left(W_P \bullet b'_{P,\alpha_{\max}} + W_S \bullet b'_{S,\alpha_{\max}}\right) + n_c \bullet \left(F_{C,\max} \bullet b\right)}{h'_{\alpha_{\max}}}$
3	$d_3 = d_{H,\max} - (F_2 - F_3)/k_{P,H,1}$	$F_3 = \dfrac{n_p \bullet \left(W_P \bullet b'_{P,\alpha_{\max}} + W_S \bullet b'_{S,\alpha_{\max}}\right) - n_c \bullet \left(F_{C,0} \bullet b\right)}{h'_{\alpha_{\max}}}$
4	$d_4 = 0$	$F_4 = \dfrac{n_p \bullet \left(W_P \bullet b'_{P,\alpha=0} + W_S \bullet b'_{S,\alpha=0}\right) - n_c \bullet \left(F_{C,0} \bullet b\right)}{h'_{\alpha=0}}$
5	$d_5 = -d_1$	$F_5 = -F_1$
6	$d_6 = -d_2$	$F_6 = -F_2$
7	$d_7 = -d_3$	$F_7 = -F_3$
8	$d_8 = -d_4$	$F_8 = -F_4$

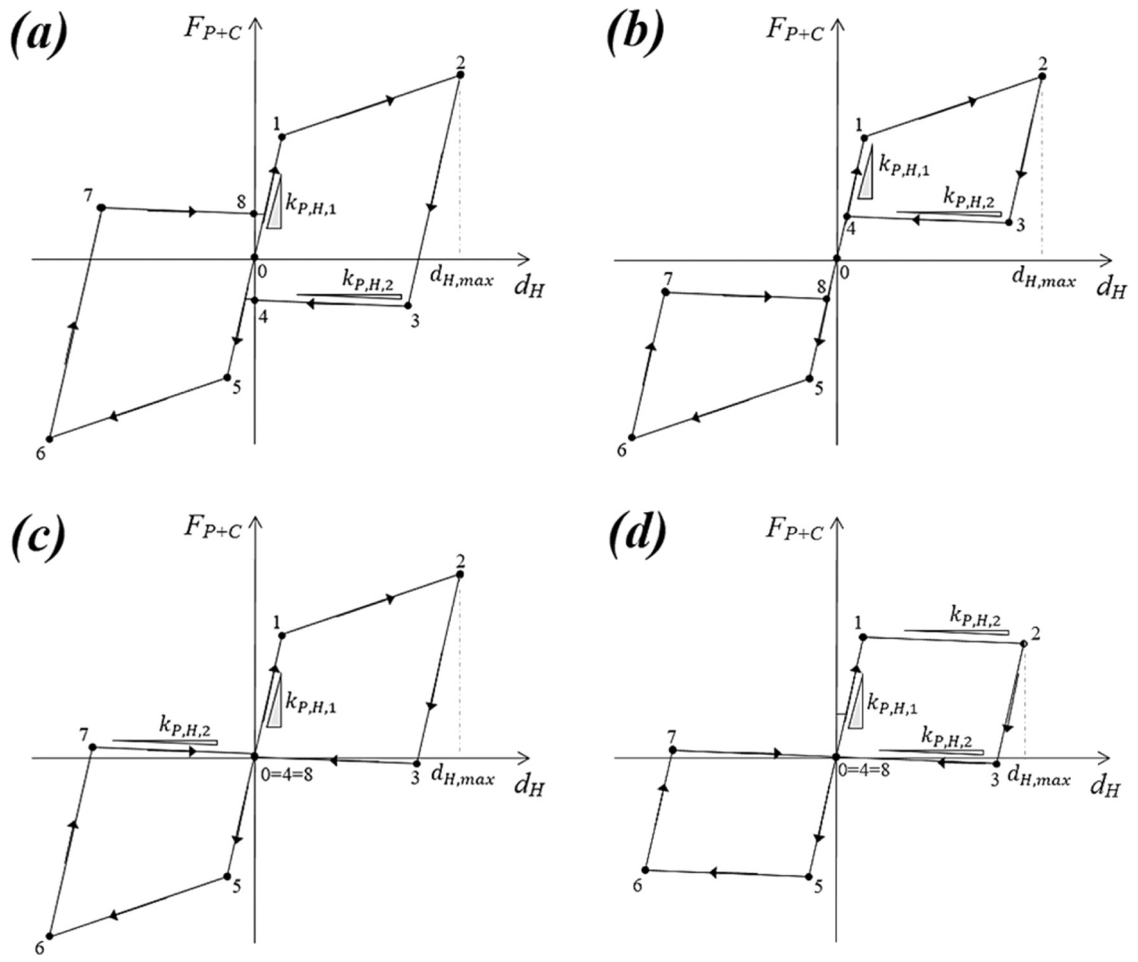

Fig. 10. Possible hysteretic responses of the dissipative rocking panels: (a) system not self-centring; (b) system self-centring; (c) system self-centring and auto-equilibrated; (d) system self-centring but unstable since featuring a negative "post-yielding" slope (i.e., $k_{P,H,2} < 0$). Refer to Table 1 for point-to-point force-displacement coordinates.

Case (d). the system behaves similarly to that of Case (c) with the only difference that here the friction connections are characterised by null "post-yielding" stiffness ($k_{C,H,2} = 0$). This is the worst case. Indeed, despite the self-centring capability (i.e., $F_3 \cong 0$ and $F_4 = 0$), the lateral strength decreases as the displacement amplitudes increase leading to an unstable system. In this case, the tangent slope from point 1 to point 2 coincides with the negative lateral stiffness (i.e., $k_{P,H,2} < 0$) of the rocking panels only. The design of the friction connections should aim to avoid this circumstance also because DBD procedures may be not reliable.

It is worth noting that all these four behaviours (Fig. 10) are easy replicable varying the design parameters of the friction connections (i.e., n_c, $F_{C,0}$ and $k_{C,2}$). However, since both the self-centring capability and a stable lateral response (i.e., positive force-displacement slope) are beneficial in seismic conditions, the design of the connections should aim to promote hysteretic loops of type-b or type-c.

4. Model validation with seismic tests of a full-scale prototype

In this section, the previously developed analytical models are validated using the results of tests carried out on a full-scale prototype of precast industrial building equipped with dissipative rocking panels installed according to the "scheme 1″ (see Fig. 3 and Fig. 6) [31]. These experiments were performed at the European Laboratory for Structural Assessment (ELSA) testing facilities of the Joint Research Centre (Ispra, Italy). Both displacement-controlled cyclic quasi-static tests and a pseudo-dynamic (PsD) test were performed. The cyclic quasi-static tests are employed hereafter to verify the proposed hysteretic models for the coupled response of rocking panels and the dissipative connections, whereas the PsD test are exploited to validate the suitability of the spectral procedure to predict the lateral response of the overall structural system under real ground motion records.

The prototype consisted of a single-storey building: 8.13 m high, made by two parallel frames (longitudinal direction) which were placed 5.0 m from one other (transversal direction), with 8.0 m bays, as shown in Fig. 11-a,b. Each frame was composed by three square columns, 500 mm side, which were inserted into pocket plinths fastened to the laboratory strong floor. They were linked to each other by two foundation beams which were bearing also a total of $6x2 = 12$ rocking panels (i.e., $n_p = 12$). Six columns supported the roof beams (750 × 500 mm) that in turn carried seven slabs (350 mm thick), with masses comparable to common buildings with this typology.

The main frame was designed for seismic actions compatible with the EC8 response spectrum for soil type B featuring a Peak Ground Acceleration (PGA) equal to 0.36 g at Ultimate Limit State (ULS, see Fig. 12-a). The rocking panels, each featuring $b = 2.5m$, $h = 8.4m$, and a cantilever lateral stiffness $k_{P,H,el} = 4.8kN/mm$, were equipped with: (i) a steel "rocking socket" at both base corners; (ii) a single dissipative friction connection capable to develop a strength $F_{C,0} = 60kN$, and a "post-yielding" slope $k_{C,2} = 2.0kN/mm$ (the structure was hence equipped with a total of ten connections, i.e. $n_c = 10$); (iii) a top connector, consisting of a steel plate with a vertical slotted hole, conceived to transmit only horizontal inertia loads. According to the "installation

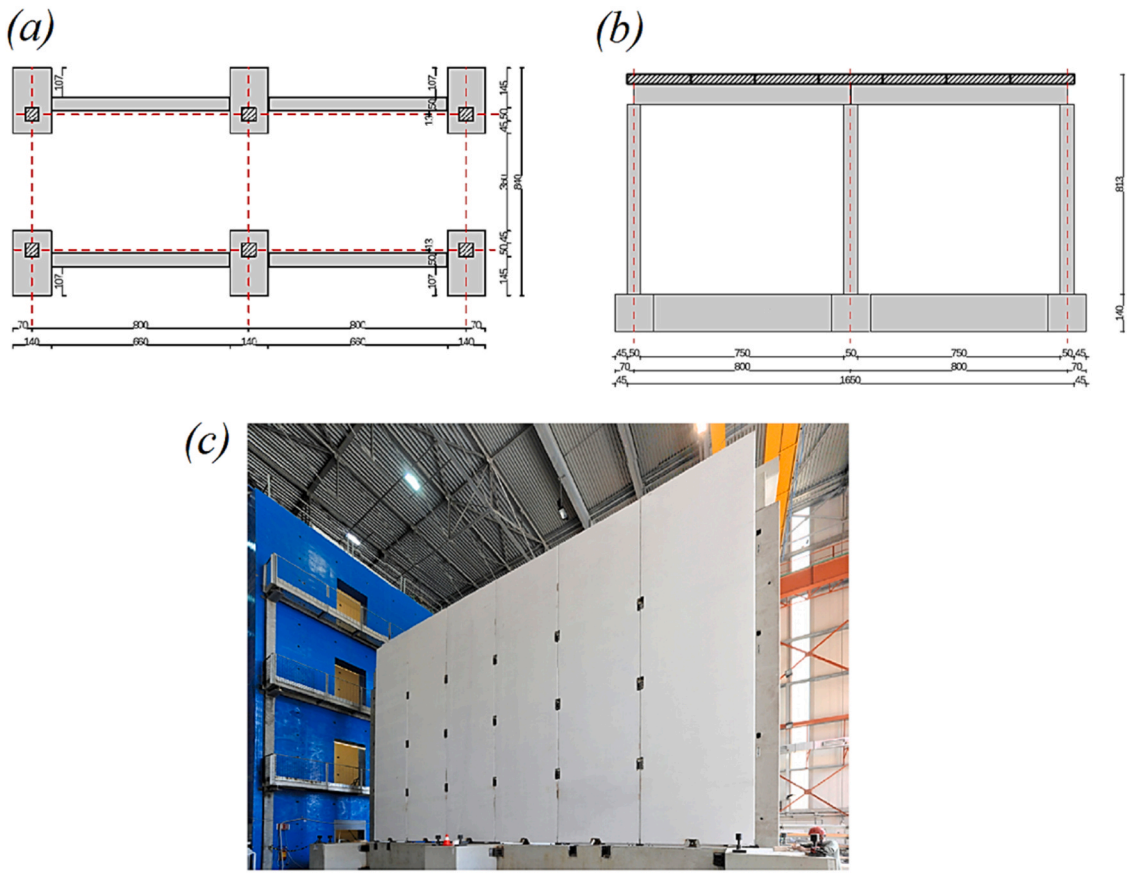

Fig. 11. Single-storey prototype building tested at the ELSA Lab: (a) planar layout, and (b) vertical section view of the main frame; (c) picture of the arrangement of the dissipative rocking panels installed along longitudinal frame.
Adapted from [31].

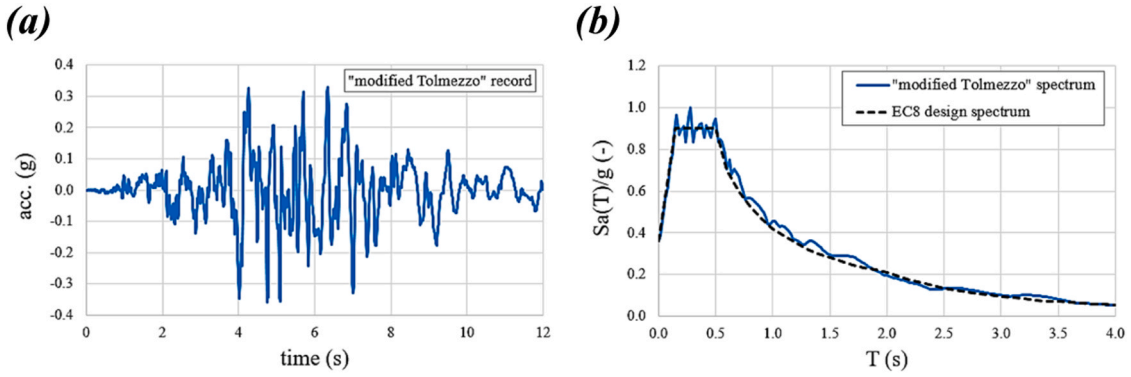

Fig. 12. Seismic input enrolled in PsD test: (a) "modified Tolmezzo" ground motion record; (b) relevant spectral matching with the EC8 design spectrum.

scheme 1″, the gravitational load of the main frame was supported by the six columns, while the rocking panels were subjected only to their self-weight. It is wort noting that the fundamental period of the bare frame (i.e., devoid of dissipative connections) was 1.53 s with a participation mass $m_1 = 170tons$ (i.e., about the whole mass of the roof plus 50 % of the mass of columns plus panels) and, as commented later for the PsD test at ULS, it was reduced by the introduction of the friction connections that increased both the damping and the lateral stiffness of the system.

Three group of tests were carried out: (1) first, a "cyclic pushover" test (test id "O1a-0″ in the referred paper), with increasing displacement amplitudes up to ± 63 mm, was carried out on the main bare frame (i.e., without panels) in order to identify its mechanical properties. It is worth noting that under the imposed maximum drift ($63mm/8130mm \cong 0.8\%$) the main frame (i.e. six columns) remained within its elastic range leading to a lateral stiffness equal to $k_{F,eff} = k_{F,el} = 2.85kN/mm$ (see Fig. 13-a); (2) the same cyclic test was later executed on the frame plus the rocking panels devoided (test id V2cb-1, see Fig. 13-b) and equipped (test id V2ca-1) with the dissipative friction connections; (3) eventually, two pseudo-dynamic (PsD) tests, one at ULS (id "V2ca-2.1″, PGA=0.36 g) and one at SLS level (id "V2ca-2.2″, PGA=0.18 g) were performed to investigate the actual seismic response of the system under real earthquakes. At ULS level, the original "Tolmezzo 1976″ (Udine, Italy) ground motion record (Fig. 12-a) was slightly modified in order to ensure the spectral matching (Fig. 12-b) with the EC8 design spectrum along with the whole range of periods (i.e., 0÷4.0 s). At SLS level, the amplitudes of the same time-history were

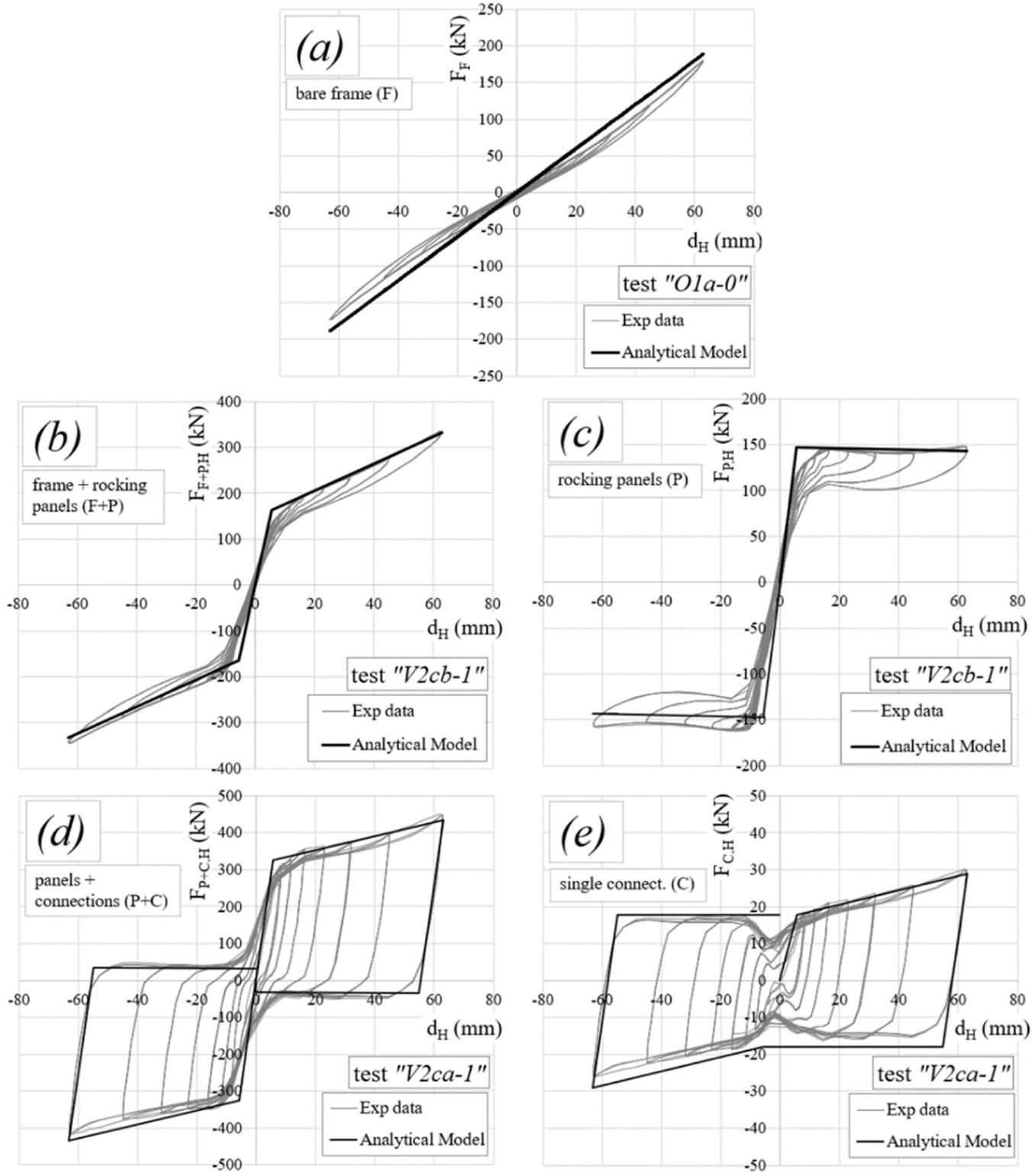

Fig. 13. Comparison between cyclic tests' data and relevant "backbone" curves obtained through analytical model: (a) main bare frame; (b) frame plus rocking panels (i.e., no dissipative connections); (c) contribution of rocking panels only; (d) rocking panels equipped with dissipative connections; (e) contribution of one dissipative connection.

scaled at 50 % (i.e., PGA=0.18 g). This allowed the Authors to perform the two PsD tests considering a single record, instead of the larger set of records prescribed by the Standard, without losing significance. Further details about the tests can be found aforementioned paper [31].

Subtracting point-to-point the elastic force of the main frame ($F_F = k_{F,el} \bullet d_H$) from relevant values recorded for test V2cb-1 and test V2ca-1″, it is possible to "isolate" the strength contribution of the twelve rocking panels ($d_H - F_{P,H}$), and equipped with the friction connections ($d_H - F_{P+C,H}$). The comparisons with the backbone F-d curves obtained through the proposed analytical models are shown in Fig. 13-c, and Fig. 13-d, respectively. For test V2cb-1″ the agreement between the analytical model and the experimental data is excellent in the positive

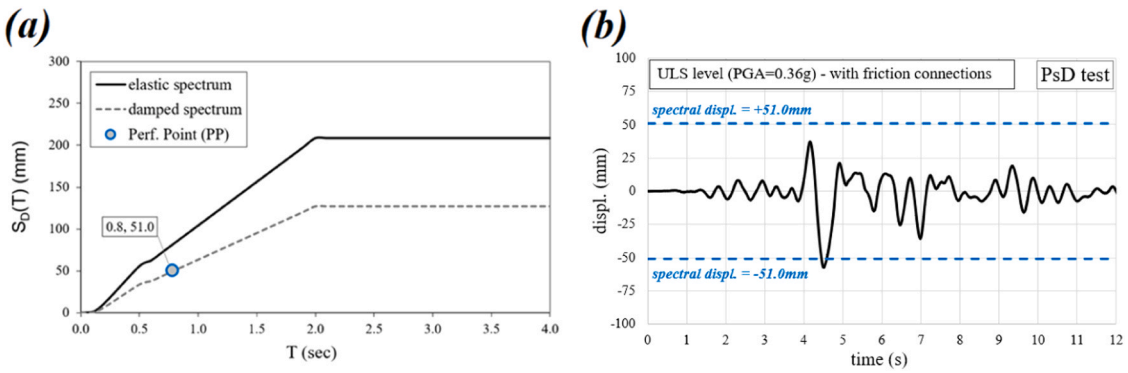

Fig. 14. Seismic response of the case-study building at ULS level: (a) maximum displacement predicted though the response spectrum analysis; (b) comparison with the displacement time-history recoded during the PsD test.

loading direction, i.e., positive displacements, both in the elastic and in the "post-yielding" field with a small discrepancy of the forces at the peak displacement (+139.6 kN vs. +147.9 kN, i.e., equal to 5.6 %). The discrepancy becomes slightly higher (−139.6 kN vs. −157.0 kN) in the opposite direction, i.e., negative displacements, where it reaches the (acceptable) value of 11.0 %. Moreover, it is surprisingly noting that this configuration of the mock-up exhibited a certain energy dissipation as witnessed by the fact that the recorded loops are not perfectly overlapped but delimitate an internal area (i.e., dissipated energy). This is most likely due to the presence, within the slotted connectors at the top of the panels, of a parasitic friction force whose contribution cannot be accounted for in analytical calculations.

The agreement between the analytical model and the experimental data was found excellent also for the test V2ca-1 during both in the elastic and in the "post-yielding" fields of the positive loading direction. The discrepancy was lower than in test V2cb-1 and identical in both loading directions, namely equal to 4.0 % (+433.2 kN vs. +451.3 kN) and 3.9 % (−433.2 kN vs. −416.8 kN), respectively. As reported in Fig. 13-e, subtracting again point-to-point the force-values of test V2cb-1 (rocking panels only, Fig. 13-c) from those of test V2ca-1 (panels with dissipative connections, see Fig. 13-d) and dividing for the total number of connections, it is eventually possible to identify, in average terms, the contribution of the single friction connection ($d_H - F_{C,H}$) to the lateral response of the structure. The analytical model is again very precise in predicting the response of the friction connection in the positive loading direction (at peak displacement, +29.0 kN vs. +30.3 kN, i.e., discrepancy 4.3 %) while, in the opposite direction, the discrepancy is larger (−29.0 kN vs. −25.6 kN, i.e., 13.3 %).

The results of the two pseudo-dynamic (PsD) tests (i.e., "V2ca-2.1″ at ULS and "V2ca-2.2″ at SLS) allow to verify the suitability of the proposed spectral procedure to predict the lateral response of single-storey buildings featuring rocking panels equipped or devoid of the aforementioned friction connections. The first condition refers to the PsD test at ULS level: the predicted (absolute) spectral displacement is $S_d\left(T_{eff}, \xi_{eq}\right) = 51.0mm$ (see Fig. 14-a), against a peak of − 57.1 mm measured experimentally (i.e., 10.7 % of error, see Fig. 14-b), being $T_{eff} = 0.78s$ the effective oscillation period, and $\xi_{eq} = 16.8\%$ the overall equivalent viscous damping (corresponding spectral reduction factor $\eta = 0.61$). See Table 2 for the complete set of the linear equivalent mechanical properties (i.e., main frame, the rocking panels, and the dissipative friction connections).

For the PsD test at SLS level, the friction connections were removed resulting in a structural system devoid of significant sources of energy dissipation (i.e., pure rocking panels) and expected to undergo larger lateral deformations. That is why, in this case, only the weak SLS seismic input was performed in order to avoid damages to both the main frame (F) and the panels (P). The relevant spectral calculation (parameters again listed in Table 2) was easily adapted by setting $n_C = 0$, i.e., number of friction connections equal to zero. The widely acceptable accuracy of the proposed analytical model is proven by Fig. 15-b that shows the comparison between peak displacement predicted though the spectral procedure and the experimental displacement-history recorded during the PsD test. In line with the previous comparison, the experimental (absolute) peak displacement of 57.6 mm, recorded at about t = 6.3 s, was only marginally higher (i.e., 10.6 %) that the relevant spectral prediction of 52.1 mm.

In this regard, it is worth noting that: (a) since for the considered single-storey frames $\Gamma_1 = 1.0$, the predicted spectral displacement corresponds to the actual lateral deformation of the real frame; (b) since during both PsD tests the main frame remained in its elastic range ($\mu_F < 1.0$), its equivalent viscous damping consisted of its elastic contribution (i.e., $\xi_{el,F} = 5\%$) and null hysteretic energy dissipation (i.e., $\xi_{F,eq} = 0\%$).

In conclusion, these achievements prove that the proposed spectral procedure, besides being simple and enough precise, can be employed for the design of single-storey buildings with rocking panels either equipped or devoid of dissipative friction connections. Future developments of this study will be focused on the extensions of this formulation to multi-storey frames also through the comparison with NLTH analyses.

Table 2
Linear equivalent mechanical properties employed for both ULS and SLS spectral calculations.

seismic level	main frame (F)		Rocking Panels (P)		Friction Connections (C)	
	$k_{F,eff}$ (kN/mm)	$\xi_{F,eq}$ (%)	$k_{P,H,eff}$ (kN/mm)	$\xi_{P,H,eq}$ (%)	$k_{C,H,eff}$ (kN/mm)	$\xi_{C,H,eq}$ (%)
ULS (PGA=0.36 g)	2.85 ($k_{F,eff} = k_{F,el}$)	0 ($\mu_F < 1.0$)	2.74	0	5.57	35.6 ($\mu_C = 9.5$)
SLS (PGA=0.18 g)	2.85 ($k_{F,eff} = k_{F,el}$)	0 ($\mu_F < 1.0$)	2.82	0	n.a.	n.a.

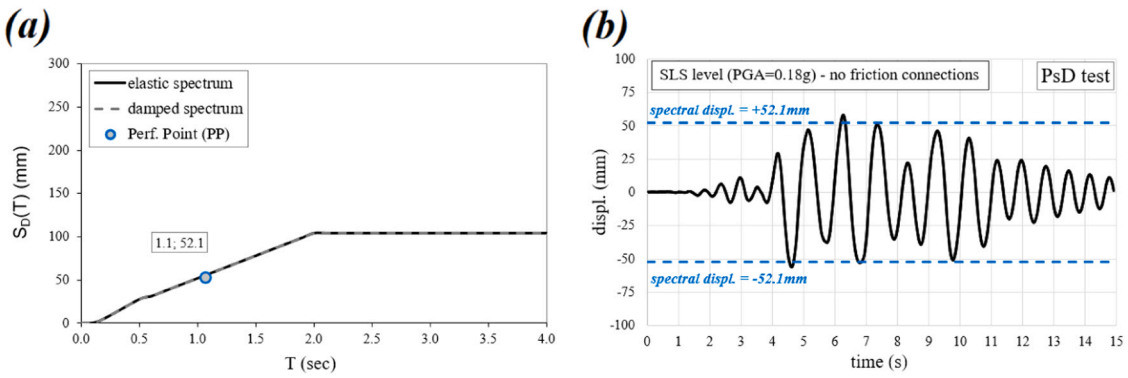

Fig. 15. Seismic response of the case-study building at SLS level: (a) maximum displacement predicted though the response spectrum analysis; (b) comparison with the displacement time-history recoded during the PsD test.

5. Conclusions

This study introduces a simplified model for rocking panels with panel-to-panel friction connections, possibly integrated with a moment-resisting frame. The resulting system exhibits force-displacement loops with significant slopes in the first and third quadrants. This allows for (i) compensation of the inherent negative stiffness in pure rocking motions, (ii) maximization of dissipated energy while maintaining self-centring capability reliant on gravity load only, and (iii) simulation of the system as a Single Degree of Freedom (SDOF) oscillator using a simplified procedure. The proposed tool was conceived to:

- simulate the response of the frame, the panels and the dissipative connections, combining all or a subset of them;
- support engineers and practitioners when calculating the seismic response of two different layouts of rocking panels (see Section 3): (1) the scheme-1 is more typical for precast concrete framed buildings with heavy-weight cladding; (2) the scheme-2 features gravity load-bearing panels without a main resisting frame as more common in modern timber buildings;
- account for the four different hysteretic responses (see Section 3.3) that can be achieved by varying the geometric and boundary conditions of the panels and the mechanical parameters of the friction connections.

The proposed method does not aim to replace more complex and accurate methods that allow the modelling of rocking systems in analytical form. It shall be applied to a single-storey building within the following limitations/assumptions:

- the rocking motion of the panels occur around a "pivot-type" rotation point (i.e., devoid of a smeared compression zone);
- while the model is capable to account for the inelastic damage of the main resisting frame, it has not been validated against this occurrence;
- accuracy may be reduced for very stiff structures with oscillation periods below 0.30 s

The procedure has been calibrated using the results of cyclic pushover and validated against results of pseudo-dynamic (PsD) tests carried out on a full-scale prototype of a precast industrial building (see Section 4). In this regard:

- the comparison with the experimental loops of the first type of tests proved a fair accuracy of the proposed hysteretic model. Indeed, maximum errors of 11.0 % and 13.3 % were detected in the quantification of the peak forces offered by the rocking panels and the friction connections, respectively;
- the results of two pseudo-dynamic tests revealed maximum difference of about 11 % between the maximum lateral displacements of the same case-study structure under the selected ground motions and the relevant values predicted through the proposed (simple) spectral calculation tool.

Future developments of this study will be focused on the extensions of this analytical tool to multi-storey frames also through the comparison with NLTH analyses. In addition, the Authors will soon publish new test results from a two-storey, full-scale Cross Laminated Timber (CLT) building, enabling validation of the simplified model with new configurations of panels and connections.

CRediT authorship contribution statement

Marco Lamperti Tornaghi: Writing – review & editing, Writing – original draft, Supervision, Investigation, Conceptualization. **Emanuele Gandelli:** Writing – review & editing, Writing – original draft, Methodology, Investigation, Data curation, Conceptualization. **Dionysios Bournas:** Supervision, Project administration, Funding acquisition.

Declaration of Competing Interest

The authors declare that they have no known competing financial interests or personal relationships that could have appeared to influence the work reported in this paper.

Data availability

Data will be made available on request.

Acknowledgments

The authors acknowledge the dedicated and careful work carried out by the Editor and Reviewers whose constructive criticism contributed to a very significant improvement of the quality of the paper.

References

[1] Aghagholizadeh M, Makris N. Response analysis of yielding structures coupled to rocking walls with supplemental damping. Earthq Eng Struct Dyn 2021. https://doi.org/10.1002/eqe.3466.
[2] Ajrab JJ, Pekcan G, Mander JB. Rocking wall-frame structures with supplemental tendon systems. J Struct Eng 2004;130(6):895–903.
[3] Bachmann JA, Vassiliou MF, Stojadinović B. Dynamics of rocking podium structures: dynamics of rocking podium structures. Earth Eng Struct Dyn 2017;46(14):2499–517. https://doi.org/10.1002/eqe.2915.
[4] Bhatta J, Dhakal RP, Sullivan TJ, Lanyon M. Low-damage rocking precast concrete cladding panels: design approach and experimental validation. J Earthq Eng 2020;26(9):4387–420. https://doi.org/10.1080/13632469.2020.1830201.
[5] Blandon CA, Priestley MJN. Equivalent viscous damping equations for direct displacement Based design. J Earthq Eng 2005;9(2):257–78.

[6] Bora C, Oliva MG, Dow Nakaki S, & D, Becker R. Development of a precast concrete shear-wall system requiring special code acceptance. PCI J 2007;52(1):122–35. https://doi.org/10.15554/pcij.01012007.122.135. 2007.

[7] Casarotti C, Monteiro R, Pinho R. Verification of spectral reduction factors for seismic assessment of bridges. Bull NZ Soc Earthq Eng 2009;42(2):111–21.

[8] Ceccotti A, Sandhaas C, Okabe M, Yasumura M, Minowa C, Kawai N. SOFIE project–3D shaking table test on a seven-storey full-scale cross-laminated timber building. Earthq Eng Struct Dyn 2013;42:2003–21.

[9] CEN, European Committee for Standardization (2004). Eurocode 8: design of structures for earthquake resistance—Part 1: general rules, seismic actions and rules for buildings, EN1998-1:2004. Bruxelles, Belgium.

[10] Christopoulos C, Filiatrault A, Folz B. Seismic response of self-centring hysteretic SDOF systems. Earthq Engng Struct Dyn 2002;31(5):1131–50. https://doi.org/10.1002/eqe.152.

[11] Dal Lago B, Biondini F, Toniolo G. Friction-based dissipative devices for precast concrete panels. Eng Struct 2017;147:356. -37.

[12] De Domenico D, Gandelli E, Quaglini V. Adaptive isolation system combining low-friction sliding pendulum bearing and SMA-based gap dampers. Eng Struct 2020;212. https://doi.org/10.1016/j.engstruct.2020.110536.

[13] Di Cesare A, Ponzo FC. Seismic retrofit of reinforced concrete frame buildings with hysteretic bracing systems: design procedure and behaviour factor. Shock Vib 2017.

[14] Englekirk RE. Design-construction of the Paramount-A 39-story precast prestressed concrete apartment building. PCI J 2002;47(4):56–71.

[15] Fitzgerald D, Miller TH, Sinha A, Nairn JA. Cross-laminated timber rocking walls with slip-friction connections. Eng Struct 2020;220:110973. https://doi.org/10.1016/j.engstruct.2020.110973.

[16] Gandelli E, De Domenico D, Quaglini V. Cyclic engagement of hysteretic steel dampers in braced buildings: a parametric investigation. Bull Earthq Eng 2021;19(12):5219–51.

[17] Gioiella L, Tubaldi E, Gara F, Dezi L, Dall'Asta A. Modal properties and seismic behaviour of buildings equipped with external dissipative pinned rocking braced frames. Eng Struct 2018;172:807–19.

[18] Hashemi A, Quenneville P. Large-scale testing of low damage rocking cross laminated timber (CLT) wall panels with friction dampers. Eng Struct 2020;206:110166. https://doi.org/10.1016/j.engstruct.2020.110166.

[19] Hashemi A, Zarnani P, Quenneville P. Seismic assessment of rocking timber walls with energy dissipation devices. Eng Struct 2020;221:111053. https://doi.org/10.1016/j.engstruct.2020.111053.

[20] Housner, G.W. (1963). The behavior of inverted pendulum structures during earthquakes. Bulletin of the Seismological Society of America. 53:403–417. doi: 10.1017/CBO9781107415324.004.

[21] Jacobsen LS. Steady forced vibrations as infuenced by damping. ASME Trans 1930;52(1):169–81.

[22] Kelly JM, Skinner RI, Heine A. Mechanisms of energy absorption in special devices for use in earthquake resistant structures. Bull NZ Natl Soc Earthq Eng 1972;5:63–88.

[23] Konstantinidis D, Makris N. Seismic response analysis of multidrum classical columns. Earthq Engng Struct Dyn 2005;34:1243–70. https://doi.org/10.1002/eqe.478.

[24] Kurama Y, Sause R, Pessiki S, Lu LW. Lateral load behavior and seismic design of unbonded post-tensioned precast concrete walls. Acids Struct J 1999;96(4):622–32.

[25] Kurama YC, Sause R, Pessiki S, Lu LW. Seismic response evaluation of unbonded post-tensioned precast walls. Acids Struct J 2002;99(5):641–51.

[26] Loo WY, Kun C, Quenneville P, Chouw N. Experimental testing of a rocking timber shear wall with slip-friction connectors. Earthq Eng Struct Dyn 2014;43(11):1621–39. https://doi.org/10.1002/eqe.2413.

[27] Makris N, Aghagholizadeh M. Effect of supplemental hysteretic and viscous damping on rocking response of free-standing columns. J Eng Mech 2019;45(5):04019028.

[28] Makris N, Konstantinidis D. The rocking spectrum and the limitations of practical design methodologies. Earthq Engng Struct Dyn 2003;32(2):265–89. https://doi.org/10.1002/eqe.223.

[29] Mazza F, Vulcano A. Displacement-based design procedure of damped braces for the seismic retroftting of RC framed buildings. Bull Earthq Eng 2015;13:2121–43.

[30] Naeim F, Kelly JM. Design of Seismic Isolated Structures: From Theory to Practice. John. Wiley & Sons; 1999. https://doi.org/10.1002/9780470172742.

[31] Negro P, Lamperti M. Seismic response of precast structures with vertical cladding panels: The SAFECLADDING experimental campaign. Eng Struct 2017;132:205–28.

[32] Ponzo FC, Di Cesare A, Arleo G, Totaro P. Protezione sismica di edifici esistenti con controventi dissipativi di tipo isteretico: aspetti progettuali ed esecutivi. Progett Sismica 2010;4:50–75.

[33] Priestley MJN, Evison RJ, Carr AJ. Seismic response of structures free to rock on their foundations. BNZSEE 1978;11(3):141–50. https://doi.org/10.5459/bnzsee.11.3.141-150.

[34] Priestley MJN, Tao JR. Seismic response of precast prestressed concrete frames with partially debonded tendons 1993;38(1):58–69. https://doi.org/10.15554/pcij.01011993.58.69.

[35] Priestly MJN, Calvi GM, Kowalsky MJ. Displacement-based seismic design of structures. 2nd ed.,. Pavia, Italy: IUSS PRESS; 2007.

[36] Psycharis IN, Lemos JV, Papastamatiou DY, Zambas C, Papantonopoulos C. Numerical study of the seismic behaviour of a part of the Parthenon Pronaos. Earthq Engng Struct Dyn 2003;32:2063–84. https://doi.org/10.1002/eqe.315.

[37] Qu Z, Wada A, Motoyui S, Sakata H, Kishiki S. Pin-supported walls for enhancing the seismic performance of building structures. Earthq Eng Struct Dyn 2012;41(14):2075–91.

[38] Rangwani K, MacRae G, Rodgers G. Performance of rocking frames with friction tension-only devices. Bull NZ Soc Earthq Eng 2023;56(2). https://doi.org/10.5459/bnzsee.1583.

[39] Wada A, Qu Z, Motoyui S, Sakata H. Seismic retrofit of existing SRC frames using rocking walls and steel dampers. Front Archit Civ Eng China 2011;5(3):259–66.

[40] Wang W, Fang C, Zhao Y, Sause R, Hu S, Ricles J. Self-centering friction spring dampers for seismic resilience. Earthq Engng Struct Dyn 2019;48(9):1045–65. https://doi.org/10.1002/eqe.3174.

[41] Yasumura M, Kobayashi K, Okabe M, Miyake T. Full-scale tests and numerical analysis of low-rise CLT structures under lateral loading. J Struct Eng (ASCE) 2016;142.

[42] Zhong C, Christopoulos C. Self-centering seismic-resistant structures: historical overview and state-of-the-art. Earthq Spectra 2022;38(2):1321–56. https://doi.org/10.1177/87552930211057581.